Journal of Sound and Vibration 396 (2017) 203–216

Contents lists available at ScienceDirect

Journal of Sound and Vibration

journal homepage: www.elsevier.com/locate/jsvi

Simulating low frequency sound transmission through walls and windows by a two-way coupled fluid structure interaction model

Finn Løvholt [a,*], Karin Norèn-Cosgriff [a], Christian Madshus [a], Ståle Engvik Ellingsen [b]

[a] Norwegian Geotechnical Institute, Computational Geomechanics, P.O. Box 3930, 0806 Oslo, Norway
[b] Brekke & Strand Acoustics, P.O. Box 1024 Hoff, 0218 Oslo, Norway

ARTICLE INFO

Article history:
Received 24 June 2016
Received in revised form
18 January 2017
Accepted 9 February 2017
Handling Editor: A.V. Metrikine
Available online 28 February 2017

Keywords:
Low-frequency sound and vibration
Two-way fluid-structure interaction
Numerical simulations
Finite element method
Structural connections

ABSTRACT

Aircraft, supersonic flights, blasts, and explosions emit sound with substantial energy below 100 Hz. When the low frequency sound is transmitted inside a building, it generates vibration and rattling that may lead to annoyance. Our understanding of these low frequency phenomena is presently limited. In this paper, we attempt to improve our computational capabilities related to the low frequency sound transmission. For this purpose, a finite element methodology that incorporates a two-way coupled fluid-structure interaction, has been developed. Results from a broad experimental investigation of low frequency sound transmission are compared with the numerical finite element simulations. Plain walls, and walls with windows are studied. Close agreement between the simulations and the laboratory measurement data is obtained in the frequency range investigated (10–100 Hz). It was found that structural connections were of large importance for modeling the vibration and sound transmission. The windows control the low frequency transmission from 15 to 30 Hz, whereas the walls control the sound transmission from 30 to 100 Hz. Mitigation of vibrations and rattling induced by low frequency sound therefore needs to consider both wall and window construction.

1. Introduction

Outdoor noise sources such as wind turbines, aircrafts, helicopters, and explosions emit sound with substantial energy in the very low frequency range below 100 Hz. The rattling due to the low frequency components of sonic booms have been subject to particular recent attention, as supersonic overland flight capabilities are presently being explored by NASA [1]. The low frequency sound may propagate efficiently to distances far from the sources [2–4]. Recent full scale tests reveal that when transmitted inside a building, the peaks of the low frequency sound spectrum correspond with fundamental acoustic room-modes [5]. In turn, the indoor sound loading generates floor vibrations, often sufficiently strong to cause human whole body vibration [6,7] as well as rattling annoyance [1]. For lightweight structures, which are studied herein, the low frequency sound also coincides with eigenfrequencies of building elements such as walls, windows, and floors, which makes it harder to mitigate their induced vibration and rattling. As a consequence, other mitigation measures are needed for low

* Corresponding author.
E-mail address: finn.lovholt@ngi.no (F. Løvholt).

http://dx.doi.org/10.1016/j.jsv.2017.02.026
0022-460X/

frequency sound and its induced vibration, compared to for instance the established methods that exists for higher frequency sound insulation. We presently lack a basic understanding and models to properly delineate the processes governing the sound transfer in this frequency range. This is naturally important towards our ability to mitigate the negative effects.

In order to improve our understanding and our ability to mitigate sound induced floor vibration, a broad research program on low frequency sound transmission into buildings and the generation of sound induced vibrations was performed between 2010 and 2016, led by the Norwegian Defense Estate Agency, and implemented by NGI (the Norwegian Geotechnical Institute). The research program comprised laboratory measurements of low frequency sound and vibration transmission through full size building elements, full-scale field tests, and the development of new numerical modeling procedures for dealing with low frequency sound transmission and vibration in buildings. More specifically, the research focused on low frequency mitigation techniques for lightweight wooden constructions. A summary of the overall project findings is found in an accompanying paper [8], whereas earlier findings are given by a series of conference papers [6,9,7]. In the present paper, we perform numerical modeling of the low frequency sound transmission through walls and windows using a Finite Element (FE) methodology, and compare the results from the numerical model with laboratory measurement data.

The attempts to model the low frequency sound transmission below 100 Hz are sparse compared to the number of studies on higher frequency sound transmission (examples comprise e.g. [10–15]). Numerical modeling of the dynamic interaction between buildings and low frequency sound dates back to studies in the seventies that made use of the Helmholtz resonator and modal decomposition approaches [16,17]. In the early nineties, Wahba [18] developed approximate eigenvalue modal decomposition techniques for estimating the fundamental structural modes for simple lightweight structures, for computing the vibration response due to a sonic boom. The modal decomposition method was later successfully validated by a Finite Element (FE) model [19]. More recently Remillieux et al., in a series of papers [14,15,20], combined modal decomposition models with geometrical acoustic methods to simulate low frequency sound transmission and sound interaction between rooms. Excellent validations with laboratory measurements [14] and finite element models [14,15] were obtained. In a related set of field experiments mimicking sonic boom sound transmission from outdoor to indoor, it was found that windows were a very important factor in the sound transfer at low frequency [21].

The bulk of existing sound transmission models are not able to properly capture the low frequency two-way interaction between the sound and the building components. However, improvements have been made recently [13–15], and particular progress on simulating the low-frequency transmission loss was obtained by Remillieux et al. [14,15]. The suggested model presented herein is aligned with these applications [13–15], and takes into account two-way fluid structure coupling and full elastic representation of the structure. The present study differs from the other studies [13–15] in the way the numerical fluid-structure interaction model is set up. To this end, this model makes use of solid elements for simulating the mechanical vibration in the structure. A new feature in the model is the use of coupling springs that take into account the behavior of the structural connections. As will be demonstrated, the detailed modeling of the lightweight constructions, including the different building components and structural connections, are needed to replicate the measured sound transmission and building response. As the handling of the structural connection properties involve some heuristic assumptions, we also discuss possible areas of modeling improvement. Furthermore, we briefly explore how the stiffness and damping properties of lightweight structures and windows affect the low frequency transmission loss for a few different types of lightweight constructions.

This paper is organized as follows: Section 2 outlines the setup, first by describing the laboratory measurements in Section 2.1, and secondly by explaining the FE methodology. In Section 3 we explore and compare the results from the numerical simulations with the laboratory measurements. The results section is split into Section 3.1 presenting the results for plain wall constructions, and Section 3.2 presenting the results for a double wall with windows. Finally we provide a short discussion of the results in Section 4, followed by a brief conclusion section.

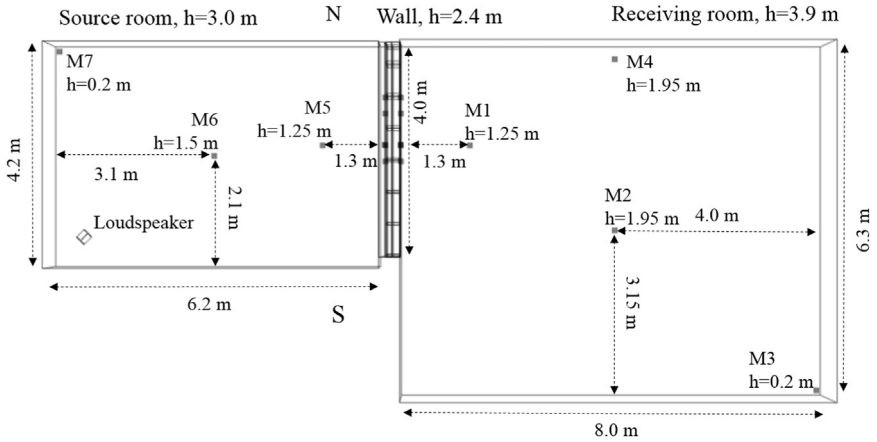

Fig. 1. Plan view of sound laboratory setup, including the locations and extent of the source and receiver rooms, the separating wall, and the locations of microphones and the loudspeaker. The drawing also represents the overall geometry defined within the numerical model in Comsol Multiphysics.

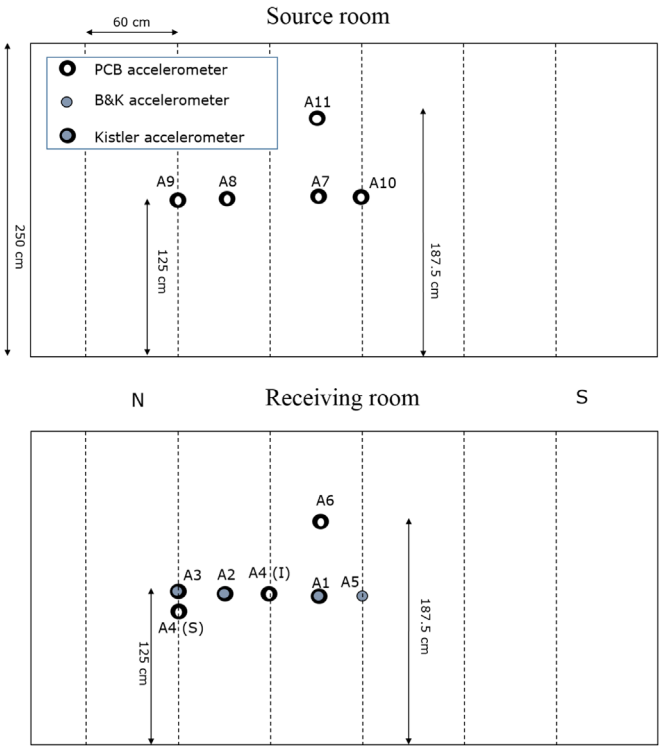

Fig. 2. Locations of accelerometers mounted on the wall surfaces for the measurements conducted in 2013, mirror view (for the walls denoted "S1" and "I1"). The upper panel shows the accelerometer locations in the source room, whereas the lower panel shows the accelerometer locations in the receiving room.

2. Experimental and numerical model setup

2.1. Laboratory experiments

The laboratory measurement program was undertaken at SINTEF Building and Infrastructure's sound laboratory in Oslo, Norway, to quantify sound transmission properties of different lightweight wooden wall structures during 2013–2014. The laboratory consists of two separate chambers made of concrete, i.e. a source room and a receiver room. The two chambers were connected through an opening where the wall structures were built (an overview is given in Fig. 1).

A sub woofer loudspeaker placed in the corner of the source room generated brown and gray noise. Three microphones were placed in the source room and four were placed in the receiver room (see Fig. 1). This includes: microphones close to the wall structure (M5 and M1), centrally in each room (M6 and M2), and in the corners (M7 and M3). The microphone types were Norsonic 1223 and Bruel & Kjær 4193. In addition, up to 14 accelerometers were glued to the wall in order to measure its vibrational response. The instrumentation differed slightly depending on whether or not a window was embedded. The locations of the accelerometers for the various structures tested are depicted in Figs. 2 and 3. The accelerometers were mirrored symmetrically on each side of the wall to as large an extent as possible. Two different types of accelerometers were used, PCB 393, and Kistler 8330A2.5. The window vibrations were measured using the lightweight Kistler accelerometers, whereas the PCB accelerometers were used elsewhere. The resulting data was compiled using a multichannel Sony data logger which served as the data acquisition system. All channels were logged simultaneously. The measurement data were stored as time series and subsequently processed with in-house signal processing software. In this paper, we focus on the low to very low frequency range between 10 and 100 Hz which is of importance for generating sound induced floor vibrations and rattling. For this reason, we removed the diffusers from the receiving room in order to provide a well controlled geometry for the numerical simulations. The signal-to-noise ratio for the sound pressure measurements room exceeded 10 dB for frequencies above 16 Hz in the receiving room.

Sound pressure and acceleration time histories were measured for a total of 16 different lightweight walls, in which some of them had windows and vents embedded. In this paper, we present the analysis of 4 out of the total of 16 structures that were tested. The construction features of each of the walls modeled herein are detailed below (see also Fig. 4 for examples of the wall and window construction and instrumentation):

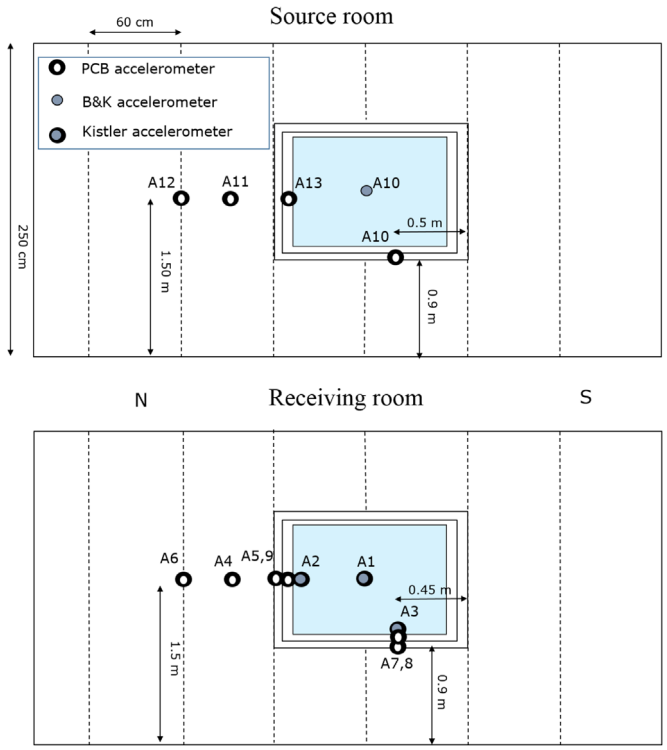

Fig. 3. Locations of the accelerometers mounted on the wall surfaces and windows for the measurements conducted in 2014, mirror view (for the walls denoted "IW1 and IW2"). The upper panel shows the accelerometer locations in the source room, whereas the lower panel shows the accelerometer locations in the receiving room.

Fig. 4. Photographs of the wall and window instrumentation. (a) shows the accelerometer positions in the source room for the standard wall (S), (b) shows the accelerometer positions in the receiver room for the improved wall (I), (c) shows the accelerometer positions in the source room for a wall with window, (d) shows the accelerometer positions in the receiver room for a wall with window.

- *S1, Standard wall:* This wall consisted of wooden studs with dimensions 48 × 148 mm, with a separation distance of 0.6 m. The 150 mm thick cavity was filled with mineral wool. On the inside, facing the receiving room, were placed one layer of 13 mm thick plaster boards. One layer of 9 mm thick plaster boards were placed on the outside facing the source room. *This wall is the standard reference wall used for comparison of the mitigating effects.*
- *I1, Improved wall:* This wall consists of wooden studs with dimensions 48 × 148 mm. The studs are stiffened by 50 × 100 mm C shaped steel sheet channel sections screwed to the studs facing outside (towards the source room). On the inside, were placed one layer of 13 mm thick plaster boards. On the outside, 22 mm thick plywood sheets were first screwed to the steel sheet profiles and secondly one layer of 9 mm thick plaster boards were attached. The 250 mm thick cavity is filled with mineral wool. *This wall is denoted the improved wall due to the increased stiffness for improved low frequency sound insulation.*
- *IW1, Improved wall with standard window:* The basic structure of was identical to I1, with the exception that the inner plaster board was replaced by 15 mm thick horizontal inner wooden paneling. A sealed double glazed windows (6 mm thick glass 12 mm thick air gap 4 mm thick glass) window with frame size dimensions 1190 × 1190 mm was placed between the two central studs (see Fig. 3 for the position). *An improved wall with standard window glazing.*
- *IW2, Improved wall with improved window:* Identical wall structure as IW1. A three layer window with frame size dimensions 1190 × 1190 mm was placed between the two central studs (see Fig. 3 for the position). The window construction comprised two laminated glasses (8.76 mm thick laminated glass, 10 mm thick gap filled with argon, 4 mm thick glass, 8 mm gap filled with argon, 8.76 thick laminated glass) *An improved wall with improved window glazing for enhanced low frequency sound insulation.*

2.2. Finite element model

The commercial finite element software package Comsol Multiphysics [22], version 4.4, was employed for simulating how the acoustic wave propagation induced structural vibrations, and, how the vibrating structure itself radiated sound back into the rooms and cavities inside the structure. The FE model is three-dimensional, incorporating the propagation of linear elastic waves and sound waves in all directions. As outlined below, it was necessary to adopt some heuristic techniques when setting up the coupled fluid-structure interaction model. In the present simulations, the geometry of the SINTEF laboratory as shown in Fig. 1 is implemented as the computational domain.

A linear frequency response analysis covering a frequency range from 10 to 100 Hz was conducted. Particular focus was given to the frequencies ranging between 15 and 30 Hz as these often coincide with the fundamental resonance frequencies of different building components such as walls, floors and windows. For wave propagation in air, the Helmholtz equation with negligible attenuation was solved. Similarly, we modeled both the insulated cavities within the studs and sheets as well as the cavities within the windows as air filled (preliminary analysis representing the cavities with mineral wool showed negligible difference). The loudspeaker was represented as a monopole source providing 1 Pa dynamic pressure for all frequencies. The model included a detailed composition of the wall structures, with three-dimensional geometries of studs, sheets, and windows. The different wall structures listed in Section 2.1 were modeled. Some building components were simplified for modeling feasibility. One such example is the C-shaped steel channel sections, which had a plate thickness of 0.7 mm. The steel channel sections were instead modeled as solid studs with a reduced elastic modulus, designed to retain the overall bending stiffness EI for normal wall deformations (see Fig. 5). However, to investigate the sensitivity due to this simplification, we also carried one simulation using shell elements to represent the C-shaped channel section (see Section 3). Another example is the laminated glass, built up with two glass panels separated by a thin film. This was represented as a compound structure in the FE model, with reduced elastic moduli representing the overall stiffness of two parallel decoupled glass sheets. The remaining structural components were modeled as isotropic linear elastic materials with frequency independent material loss factors. All the material parameters are listed in Table 1. The selection of the elastic parameters was based on standard references [23]. However, some parameters were adapted during the simulations. For instance, material damping factors were increased in the simulations in order to achieve satisfactory agreement with observations. Properties for compound structures, such as the wooden paneling used in IW1 and IW2, were also subject to tuning.

Fluid-structure-interaction was modeled by imposing the dynamic air pressure as a normal force acting on all exposed structural surface boundaries. Likewise, continuity of particle acceleration along the boundaries interfacing the structure

Table 1
Material parameters used for the finite element simulations.

Component	E [GPa]	ν	ρ [kg/m^3]	η
Stud	7	0.05	500	0.1
Steel section (equivalent)	5.4	0.33	200	0.1
Plasterboard	4	0.33	800	0.1
Wooden paneling	7	0.05	500	0.1
Plywood	10	0.05	550	0.1
Glass	60	0.33	2500	0.025
Laminated glass (equivalent)	15	0.33	2500	0.1

Table 2
Coupling spring parameters used for the finite element simulations.

Wall	Stud-plasterboard Stud-steel Plasterboard-plywood		Steel-plywood Plasterboard-inner paneling		Window-frame	
Direction	Normal	Tangential	Normal	Tangential	Normal	Tangential
S1	7.5	750	NA	NA	NA	NA
I1	7.5	750	3.75	375	NA	NA
IW1	5	500	2.5	250	0	90
IW2	5	500	2.5	250	0	90

and fluid was ensured (Fig. 5). The concrete wall boundaries inside the source and receiving rooms were assumed to be fully reflecting. Two Comsol modules, “acoustics” and “structural mechanics”, in Comsol Multiphysics 4.4, were employed for this purpose. Quadratic Finite Elements were employed for both the fluid (air) domain as well as for the linear elastic material. The mesh consisted of adaptive tetrahedra-shaped elements. Due to the need to resolve the thin structures (windows and thin sheets), the sizes of the elements could vary significantly. Typical constraints for the maximum and minimum element dimensions were set to 0.5 m and 0.1 m respectively, while smaller element dimensions were needed across the smallest dimensions of the windows and sheets. The meshing typically resulted in $250–500 \cdot 10^3$ degrees of freedom, the largest models were those that included windows. A PARDISO solver was used for solving the linear system. Grid refinement tests were conducted to ensure a reasonable convergence in the applied frequency range.

In preliminary simulations it was crudely assumed that the connections between different structural parts were monolithic. This means that the stresses and displacements between the different elastic materials in the walls and windows were continuous, leading to restrained motion of each structural component. However, by comparing the preliminary results with measurement data, it was found that the dynamic stiffness for this configuration was much too high compared to the measurements (see Section 3). Therefore, linear 2D elastic coupling springs representing the structural connections (e.g. between sheet-sheet, stud-sheet, stud-window) were introduced. The stiffness of the coupling springs were largest along the tangential direction compared to the normal direction. The edges of the sheets and studs were simply supported along the boundary to the laboratory concrete walls, whereas the respective surfaces facing the boundary were free. Brief analysis of the eigenfrequencies was conducted for certain structures [24], which revealed that the walls behaved like simply supported structures with Young's Moduli of 7–8 GPa; an observation that was used in the FE simulations. The properties of the coupling springs were determined in an iterative manner, by comparing the simulations with measurement data and adjusting the parameters to minimize offsets (the parameters are listed in Table 2). The simulations and the parameter choices presented in this paper only represent a small subset of the total number of simulations. A large set of simulations were carried out initially in order to tune the model parameters and

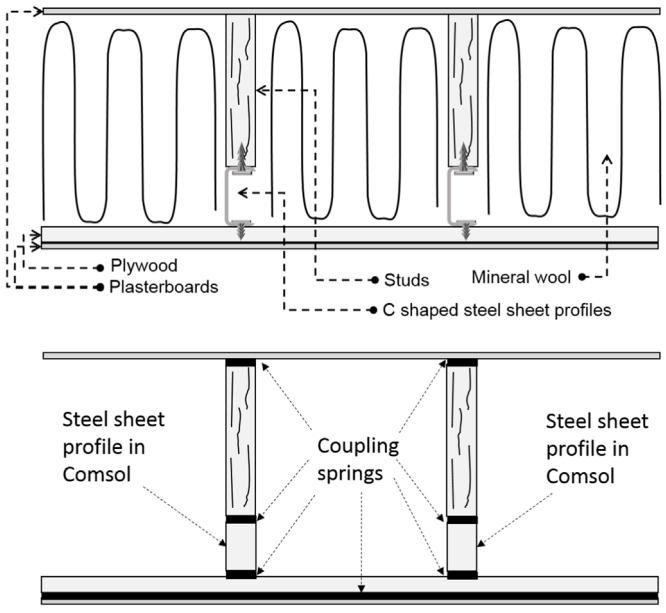

Fig. 5. Sketch showing the cross section of wall “I1” in a horizontal plane, comparing the wall as built and with simplifications implemented in Comsol. Upper panel, principle sketch of the structure as built. Lower panel, the same structure as modeled in Comsol. The black rectangles indicate the locations of the coupling springs. While these are infinitely thin in the real model, they are enlarged here for increased visibility.

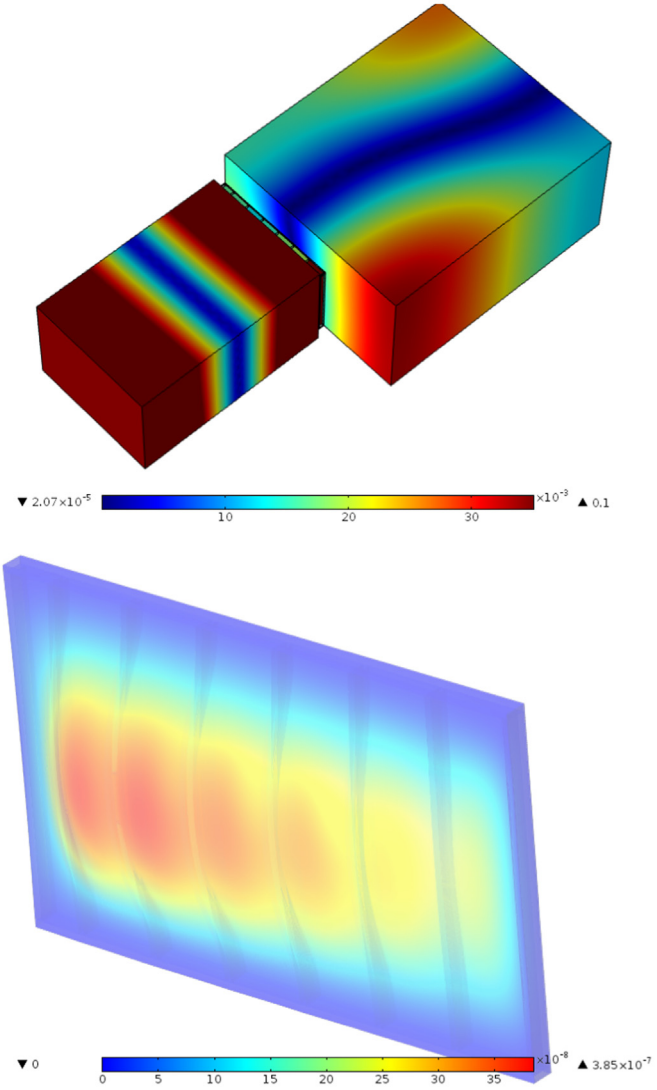

Fig. 6. Example of the calculated sound pressure and wall deformations using Comsol Multiphysics. The present example is for S1 (the standard wall) at 25.11 Hz. Upper panel: Calculated absolute sound pressure, the colorbar represents the absolute sound pressure in Pa. Lower panel: wall vibration deformation pattern, the colorbar shows a normalized horizontal displacement. (For interpretation of the references to color in this figure legend, the reader is referred to the web version of this article.)

constraints, including sensitivity studies of the parametric values for the structural connections and the mounting of the walls. While the results from these sensitivity studies are not included here, we note that results from parts of the analysis can be found in a M.Sc. Thesis [24] (in Norwegian).

3. Results

The FE model described in Section 2.2 was used to simulate the coupled elastic-acoustic wave propagation for the wall constructions S1 and I1 (Section 3.1), and for the wall-window structures IW1 and IW2 (Section 3.2). To demonstrate the methodology, we present results for the plain walls in detail first, while we focus only on the most important results for the walls with windows.

Generally, results are presented in terms of transmission losses or admittances. We define the transmission loss as

$$\Delta L_p = 20\log 10\left(\frac{|p_{re}|}{|p_{so}|}\right) \tag{1}$$

and the admittance as

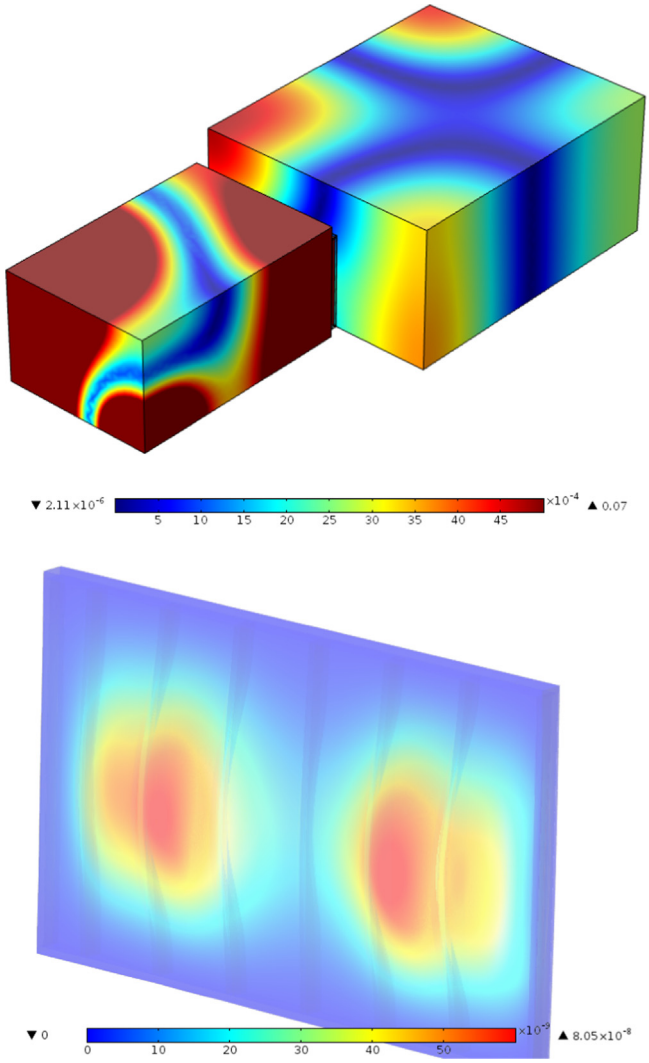

Fig. 7. Example of the calculated sound pressure and wall deformations using Comsol Multiphysics. The present example is for S1 (the standard wall) at 34.97 Hz. Upper panel: Calculated absolute sound pressure, the colorbar represents the absolute sound pressure in Pa. Lower panel: wall vibration deformation pattern, the colorbar shows a normalized horizontal displacement. (For interpretation of the references to color in this figure legend, the reader is referred to the web version of this article.)

$$\beta = \frac{|\dot{u}_n|}{|p_{so}|} \tag{2}$$

The different quantities above are the absolute values of the pressures $|p_{re}|$ and $|p_{so}|$ in the receiving room and the source room, respectively. Unless otherwise stated, the absolute pressures are arithmetic means of M1-3 (receiving room), and M5-7 (source room). Likewise, the admittances are derived from the absolute normal velocity $|\dot{u}_n|$ point values at given sensor positions shown in Figs. 2 and 3, using $|p_{so}|$ as the reference pressure. The transmission loss is given in dB and the admittance in mm/s/Pa.

3.1. Acoustic pressure and admittance for the plain walls

Figs. 6 and 7 show examples of simulated absolute sound pressure fields and the wall displacement patterns for the standard wall S1. Results are depicted for frequencies $f=25.11$ Hz and $f=34.97$ Hz respectively. Fig. 6 shows that the acoustic pressure field in the emitting room for $f=25.11$ Hz is close to the fundamental room eigenmode, evident from the standing wave pattern and the pressure anti-node located centrally. The wave pattern in the receiving room, coupled to the source room via the vibrating wall, exhibit a more asymmetric pattern with higher pressures in two opposite corners. Correspondingly, wall displacement is characterized by a combination of uniform bending of the wall and individual deformations for the plasterboard sheets between

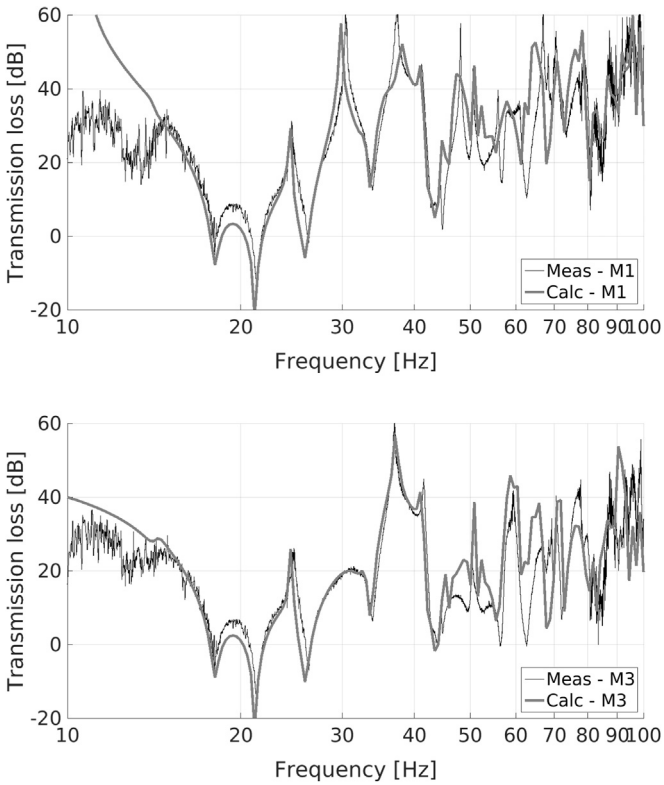

Fig. 8. Measured and calculated transmission losses for I1 (the improved wall) at individual microphone positions M1 and M3 in the receiving room (see Fig. 1). Microphone M7 is used as the reference pressure. The upper panel shows results for M1, the microphone closest to the wall. The lower panel shows results for M3, the corner microphone.

each of the wooden studs. Furthermore, the displacements are slightly larger on the left hand side of the wall. For $f=34.97$ Hz, a more complex sound propagation field is evident. The location of the simulated anti-node is clearly affected by the location of the sound source in the nearest corner, but apart from that it lacks a clearly identified pattern. A standing wave field with the largest pressure in all four corners of the receiving room, as well as plus-shaped pressure anti-node in the center of the room are present in the receiving room is apparent. The wall displacement field for $f=34.97$ Hz exhibits a shorter wavelength with two distinct sections constituting the main part of the wall deformation. At higher frequencies, the wall deformation pattern and room modes become increasingly more complex (results not shown).

Fig. 8 shows simulated transmission losses for the two individual microphone positions M1 and M3 in the receiving room for I1. A similar comparison for S1 is given in Fig. 9. In these comparisons, the sound pressure measured or simulated at M7 (source room corner) is used as the reference pressure. We first focus on the upper panels that depict the transmission losses close to the wall (M1). For I1, the simulations fit well with the measurements near the wall, both for the lowest and the highest frequencies investigated. The simulations tend to predict lower transmission losses than the measurements at the lowest frequencies. For S1, a clear discrepancy between the simulations and measurements for the very lowest frequencies is observed near the wall (we note that low signal-to-noise-ratios are present below 15 Hz), whereas the agreement is better above 30 Hz. This offset between measurements and observations for S1 and M1 below 30 Hz is generally not seen for the other structures tested (not all results are shown), and the simulations mainly follow the trends from the measurements.

The corner microphones are needed in low frequency measurements as they are less sensitive to the room's standing wave pattern at low frequency, which is evident from Figs. 6 and 7. The lower panels shown in Figs. 8 and 9 present the results for the corner microphone (M3). Close correspondence between the measurements and simulations from 15 Hz to 70 Hz for both I1 and S1 is observed. For the standard wall, the agreement at the corner microphone position is clearly better than for the microphone position near the wall, particularly below 30 Hz. For I1, the main discrepancy between the modeled and measured transmission loss is near 65 Hz, which is likely due to the double wall resonance (theoretically 58 Hz for I1, but likely higher in reality as the studs makes the response stiffer). We also obtain a similar fit between simulations and measurements for other constructions (results not shown).

As noted in Section 2.2, agreement between simulations and measurements were obtained by systematically varying the stiffnesses of the coupling springs, focusing on the resulting corner-corner microphone transmission losses. The first simulation was conducted without the coupling springs, meaning that the joints between the construction elements were monolithic. The result from this simulation is shown with a dashed line in the lower panel of Fig. 9. This monolithic structure provided much too high transmission losses for the majority of the frequencies investigated.

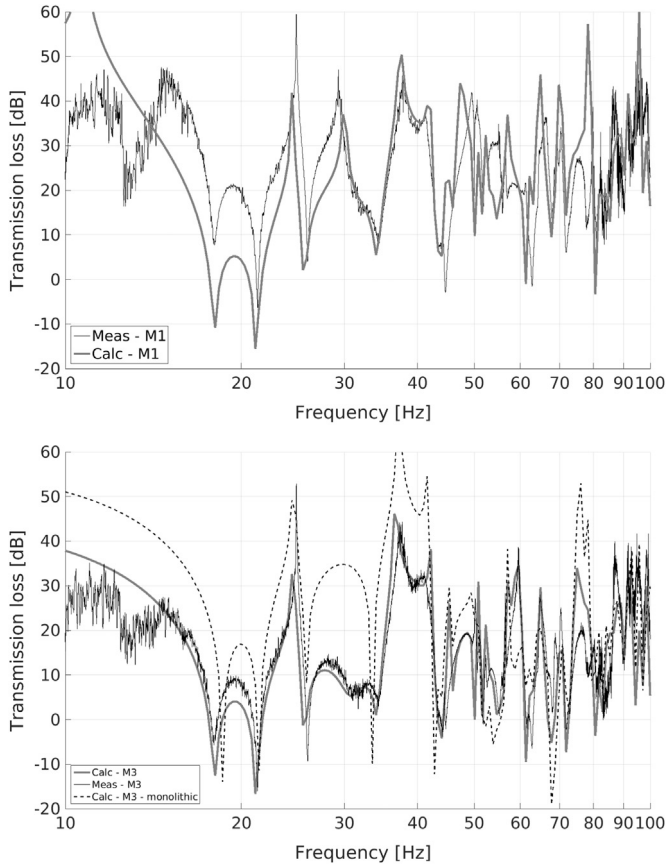

Fig. 9. Measured and calculated transmission losses for S1 (the standard wall) for microphone positions M1 and M3 in the receiving room (see Fig. 1). Microphone M7 is used as the reference pressure. The upper panel shows results for M1, the microphone closest to the wall. The lower panel shows results for M3, the corner microphone. In the lower panel, the result from a calculation using a monolithic wall (i.e. with totally stiff connections between the building components), is also shown.

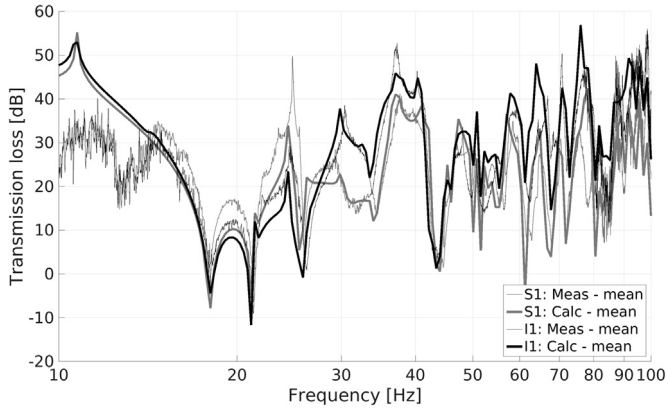

Fig. 10. Measured and calculated transmission losses for S1 (the standard wall) and I1 (the improved wall). The transmission loss is defined as the arithmetic mean value of sound pressure in emitting room (M5-7) divided by the sound pressure in the receiving room (M1-3).

Fig. 10 shows the transmission losses computed by the arithmetic mean pressure (as defined in Eq. (1)) for S1 and I1. For S1, the simulations generally fit the data well over the whole frequency spectrum, apart from a slight deviation in the lowest frequency range, primarily due to discrepancies at position M1. Differences between simulations and measurements for M2 gave rise to the slight deviation near 25 Hz. Above 70 Hz say, the agreement with the measurements are worse than for the lowest frequencies. For I1, we obtain better correspondence with the observations. Fig. 10 further shows that larger transmission is observed for I1 than for S1 above 30 Hz, but that we get larger

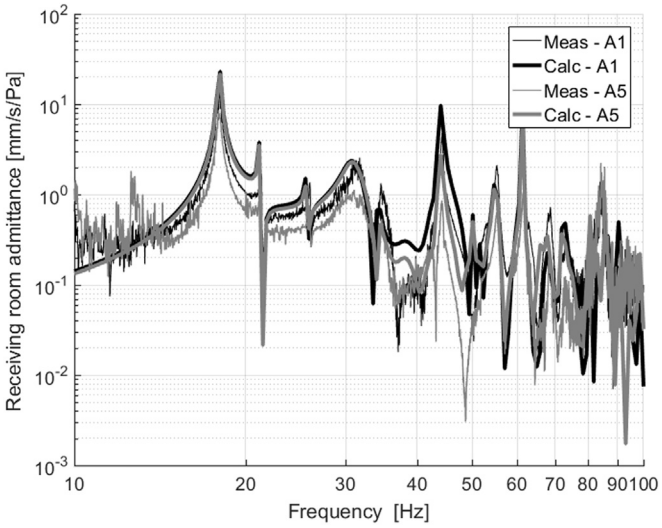

Fig. 11. Measured and calculated wall admittances for sensor positions A1 (center of plate) and A5 (located on stud) for S1 (the standard wall).

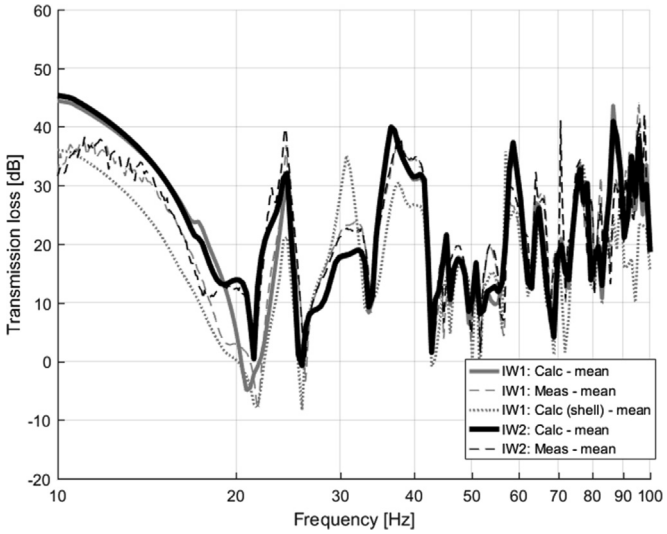

Fig. 12. Measured and calculated transmission losses for IW1 (the improved wall with standard window) and IW2 (the improved wall with improved window). The curve denoted with "shell" indicates that shell elements are used for modeling the C-shaped profiles. The curves represent arithmetic mean values of the sound pressure in emitting room (M5-7) divided by the sound pressure in the receiving room (M1-3).

transmission losses for S1 at the very lowest frequencies. One possible reason for the lack of improved transmission loss for the lowest frequencies for I1, may be the low torsional stiffness of steel channel sections. Fortunately, as explained below, the worsened transmission loss in this frequency range did not prove crucial in the overall attempt to mitigate the very low frequency sound transmission.

Fig. 11 compares the simulated admittances for the standard wall S1 for accelerometer positions A1 (located between two studs) and A5 (located on the stud) in the receiving room (similar overall trends are found for I1). Here, microphone M7 is used for defining the reference pressure. The simulated admittances follow the main trends from the measurements, and the locations of the individual peaks and troughs in the transmission loss spectrum are captured well. For the lowest frequencies, the admittance for A1 gives the best agreement with the observations, whereas A5 gives the better fit above 30 Hz or so. Generally, there is a gap between A1 and A5 in the measurements that are not clearly distinguished in the lowest frequency range. However, the admittance curves have a clear separation in the 35–50 Hz range. This might be related to the simulated double wall resonance, as this is the only place the admittance curves at the stud and at the center of the sheet separate clearly.

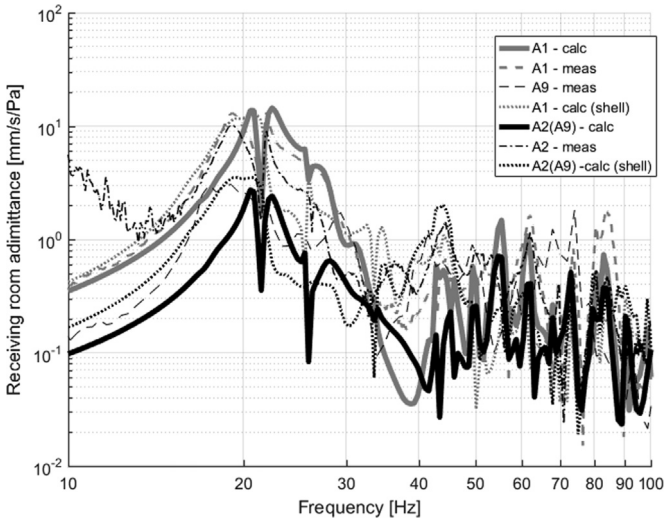

Fig. 13. Measured and calculated wall admittances for sensor positions A1 (window center), A2 (window edge), and A9 (window frame) for IW1 (the improved wall with standard window). The curve denoted with "shell" indicates that shell elements are used for modeling the C-shaped profiles.

3.2. Acoustic pressure and admittance for the walls with windows

Fig. 12 shows transmission loss using the arithmetic mean pressures (as defined in Eq. (1)) for both the improved walls with windows (IW1 and IW2). Excellent agreement between the simulations and measurements is observed, the simulations follow the main trends of the measured transmission loss spectrum. Importantly, it is noted that the results for IW1 were obtained without any change in heuristic assumptions , but by straightforwardly employing the best fit coupling spring stiffnesses from IW2. One simulation using a shell element for the C-shaped profile for comparison (shown with a dotted line in Fig. 12) was performed. While this simulation also follows the trend of the measurement, the general agreement is not as good as for the best fit solution shown with the solid line. On the other hand, the simulation employing the shell element seems to fit better at the lowest frequencies. This becomes even clearer when we inspect the simulated admittances (see below). While the main trends are captured over the full frequency range, the best agreement is obtained between 35 and 80 Hz. Above 25 Hz, the transmission losses are identical for both walls, implying that the wall construction rather than the window is controlling the sound transmission over this frequency range. However, in the frequency range covering approximately 17–25 Hz, which is the most important range for generating floor vibrations, we find that the window properties primarily control the sound transmission. Over this particular frequency range, the improved windows increased the transmission loss, particularly due to increased damping. Measurements and simulations on other wall-window constructions included in the laboratory tests consolidate this finding (results not shown). Finally a slight offset is observed between the asymptotic behavior in the measurements and the simulations for the lowest frequencies.

Fig. 13 shows the measured and simulated admittances at the window center and along the window edges for IW1. Microphone M7 is used for establishing the reference pressure. We compare first the admittance at accelerometer position A1 located centrally at the window. At low frequencies, the simulations follow the measurements up to about 35 Hz, while there are more pronounced discrepancies at higher frequencies. However, the similar transmission losses for IW1 and IW2 indirectly suggest that the window dynamics are of less importance for the sound transmission at higher frequencies. Next, we compare the simulated window admittance at the measured accelerometer locations A2 and A9 with the simulated accelerometer location A2. As shown in Fig. 3, these two accelerometers are located close to each other. While the simulated and measured admittances are fairly similar, the measurements generally show higher vibrations than the simulations. A flat peak in the measured admittance that extend to lower frequencies than in the simulated admittance is also observed. It is further noted that the simulations at point A2 are more similar to the measurements at A9 than A2. In the measurements, the admittance increases linearly from accelerometers A9 to A2 (from the window frame to the window center). This implies that the window frame is more mobile in the measurements than in the simulations. This discrepancy between the measured and simulated admittances is most likely the reason for the offset in transmission loss at 17–18 Hz observed in Fig. 12. To this end, it is noted that simulations carried out using the shell elements for the C-shaped steel profiles seem to fit better towards the admittances, particularly for the flat peak below 20 Hz, which is also reflected in the improved match for the transmission loss below 20 Hz.

4. Discussion

For modeling the transmission loss for frequencies below 100 Hz, including the two-way interaction between the sound fields of the rooms, cavities and the elastic motion of the structures were needed. In the model, the structural connection properties are crucial for simulated the sound transmission. In the first FE models for the lightweight walls, the structural connections between studs and sheets were modeled as monolithic, leading to excessive transmission losses. To remedy, we included a set of coupling springs between the different building elements. By altering the numeric values of the coupling springs, the simulations matched closely the measured transmission losses between the emitting and the receiving rooms in our simulations, and to some extent the wall admittances. As a consequence, the present investigation hints that a detailed representation of the structural connections between the structural elements may be needed in the model.

Despite the good agreement between the model and the measurements, the model could still be refined. In particular, the measured differences between the sheet and stud admittances are not fully captured in the simulations. Similarly, the motion of the different window frames and edges are not fully captured. Still, the simulations using shell elements to represent the C-shaped profiles holds promise that future analysis with more accurate representation of the structure may improve our models. To improve the situation, two different pathways should be investigated: Measurements of the dynamic properties of the walls and windows revealing the fundamental frequencies of the compound walls may be used to better characterise the dynamic stiffnesses and material parameters of the structures. While brief analysis of the eigenfrequencies was conducted for certain structures [24] a systematic quantification of the dynamic properties of the walls and studs for all configurations was not conducted. Remillieux [14] used measurements to derive the modal characteristics of the structure to determine the basic modal properties of the wall. With such measurements at hand, more rigorous treatment of the different connections and mount points could be performed, and used to updated the model parameters. We suggest to model the mounting and support of the different plywood, plasterboard, and panels in more detail, taking into account the location of each individual plate and structure. We note also that some structural components could be modeled more in detail, for instance using shell elements for the C-shaped profiles throughout, or representing the anisotropic properties of the studs and sheets.

The measurements have further illuminated sound insulation properties of two types of mitigation measures towards very low frequency sound insulation, firstly by improving the wall stiffness, and secondly by improving the window damping. While the practical aspects related to the mitigation measures are mainly treated in an accompanion paper [8], a couple of key remarks are given: The increased wall stiffness provided better sound insulation for frequencies of 30 Hz and higher, but unfortunately a worsened situation in the frequency range between 15 and 30 Hz that is crucial for inducing floor vibration. However, it was found that in this frequency range, the windows control the low frequency sound transmission. By replacing a standard two-layer window with a three layer window with two laminated glass sheets, improved transmission losses were obtained. The FE model results suggest that this was due to increased material damping due to the lamination. The same model has also been used to explore how changes in material properties for other windows affected the transmission losses. Altogether, the combination of an improved wall stiffness combined with improving the window provides better sound insulation properties at low frequency. This is further verified by the extensive full scale field tests [8] where the implementation of the countermeasures were combined and tested for a building.

5. Conclusion

A procedure for simulating the sound transmission at low-to-very-low frequencies has been developed and tested for a set of lightweight walls with and without windows. The method is primarily designed for simulating structural low frequency indoor sound transmission, for a frequency range where sound induced secondary rattling and indoor floor vibrations occur. Close agreement with results from low frequency sound and vibration laboratory measurements from 10 to 100 Hz were obtained. The level of correspondence depends on the construction type and the particular frequency band investigated. The employed method may potentially fill a gap in a frequency range were there previously has been a lack of reliable procedures for calculating the effectiveness of sound insulation.

Only one previous study [14] has been found that was able to reproduce measured low-frequency sound transmission and dynamic response to similar accuracy as demonstrated herein. Compared to [14], the present paper also demonstrates how various lightweight constructions and windows differ with respect to their low frequency response. To our knowledge, our study significantly extend previous understanding by addressing complex features of two-chamber coupling, including the interaction of fundamental acoustic and structural harmonics at low eigenfrequencies, that have not previously been calculated accurately at the low frequencies in question. Detailed modeling of structural connections were needed to match simulations and measurements. However, as discrepancies are still present, future model amendments related to the handling of joints and structural support are likely to provide model improvements and transparency. To this end, methodologies adopted from modal characterisation [14] represent a suitable alternative, to improve the characterization of the dynamic structural properties.

Acknowledgements

This work was financially supported by the Norwegian Defence Estate Agency and NGI. This support is highly acknowledged. We thank Klaus Tronstad and Ole Espen Buer at NGI for carrying out the laboratory measurements. The authors further thank Arild Brekke at Brekke & Strand Acoustics, for his suggestions towards the design of the different walls tested, as well as technical advise for detailing the measurement setup in the laboratory. Vaughan Meyer is thanked for proofreading a revised version of the paper with respect to English grammar. An anonymous reviewer is thanked for constructive comments that improved the quality and clarity of the paper. Finally we thank Halvard Høilund-Kaupang and Sigurd Hveem at SINTEF Building and Infrastructure, for their technical assistance as well as for allowing use of their laboratory.

References

[1] J. Rathsam, A. Loubeau, J. Klos, Effects of indoor rattle sounds on annoyance caused by sonic booms, J. Acoust. Soc. Am. 138 (1).
[2] E. Salomons, *Computational Atmospheric Acoustics*, Kluver Academic Publishers, Dordrecht, 2001.
[3] C. Madshus, F. Løvholt, A. Kaynia, L. Hole, K. Attenborough, S. Taherzadeh, Air-ground interaction in long range propagation of low frequency sound and vibration – field tests and model verification, *Appl. Acoust.* 66 (2005) 553–578.
[4] K. Attenborough, K. Li, K. Horoshenkov, *Predicting Outdoor Sound*, Taylor & Francis, London & New York, 2007.
[5] F. Løvholt, C. Madshus, K. Norén-Cosgriff, Analysis of low frequency sound and sound induced vibration in a Norwegian wooden building, *Noise Control Eng. J.* 59 (4) (2011) 383–396.
[6] F. Løvholt, K. Rothscild, C. Madshus, K. Tronstad, Building vibration generated by low frequency sound from blasts and Aircrafts, in: Proceedings of INTER-NOISE and NOISE-CON Congress and Conference Proceedings, vol. 7, Ottawa, Canada, 2009, pp. 58–66.
[7] F. Løvholt, K. Norén-Cosgriff, C. Madshus, A. Brekke, On the low frequency sound transmission and induced vibration from aircrafts, in: Proceedings of INTER-NOISE and NOISE-CON Congress and Conference Proceedings, vol. 247, Insbruck, Austria, 2013, pp. 2898–2905.
[8] K. Norén-Cosgriff, F. Løvholt, A. Brekke, C. Madshus, H. Høilund-Kaupang, Countermeasures against noise and vibrations in lightweight wooden buildings caused by outdoor noise sources with strong low frequency components, *Noise Control Eng. J.* 64 (1) (2016) 737–752.
[9] F. Løvholt, C. Madshus, K. Norén-Cosgriff, Low frequency sound generated vibration in buildings due to military training and air traffic, in: Proceedings of INTER-NOISE and NOISE-CON Congress and Conference Proceedings, vol. 6, Lisbon, Portugal, 2010, pp. 4551–4560.
[10] K. Martini, J. Garrelick, Computation of the response of a window embedded in a 3-D enclosure to a sonic boom using FE/BE techniques, *Comput. Struct.* 65 (3) (2009) 395–401.
[11] S. Maluski, B. Gibbs, Application of a finite-element model to low-frequency sound insulation in dwellings, *J. Acoust. Soc. Am.* 108 (4) (2000) 1741–1751.
[12] P. Jean, Sound transmission through opened windows, *Appl. Acoust.* 70 (1) (2009) 41–49.
[13] A. Jessop, K. Li, J. Bolton, Reduction of low frequency noise transmitted through a single-pane window, *Acta Acoust.* 97 (2011) 382–390.
[14] M. Remillieux, External pressure loading vibration and acoustic responses at low frequencies of building components exposed to impulsive sound, *Appl. Acoust.* 73 (2012) 1059–1075.
[15] M. Remillieux, S. Pasareanu, U. Svensson, Numerical modeling of the exterior-to-interior transmission of impulsive sound through three-dimensional thin-walled elastic structures, *J. Sound. Vib.* 332 (2013) 6725–6742.
[16] P. Vadiya, The acoustic response of rooms with open windows to airborne sound, *J. Sound. Vib.* 25 (4) (1972) 505–532.
[17] P. Vadiya, The transmission of sonic boom signals into rooms through open windows, *J. Sound. Vib.* 25 (4) (1972) 533–559.
[18] N. Wahba, Analysis of a plaster-wood wall using a series solution, *Comput. Struct.* 35 (2) (1990) 121–140.
[19] N. Wahba, Analysis of a plaster-wood wall using a finite-element method, *Comput. Struct.* 36 (4) (1990) 743–753.
[20] M. Remillieux, R. Burdisso, G. Reichard, Transmission of sonic booms into a rectangular room with a plaster-wood wall using a modal–Interaction model, *J. Sound. Vib.* 327 (2009) 529–556.
[21] T. Haac, J. Corcoran, G. Remillieux, M.C. Reichard, R. Burdisso, Experimental characterization of the vibro-acoustic response of a simple residential structure to a simulated sonic boom, in: Proceedings of AIAA/CEAS Aeroacoustics Conference, vol. 15, Miami, Florida, USA, 2009.
[22] Comsol Multiphysics Web Page, 2016.
[23] Byggforsk, Lyddate for materialer og konstruksjoner, Tech. Rep. 573.420, Byggforskserien, in Norwegian, 1996.
[24] S. Ellingsen, Numerisk beregning av lavfrekvent lydtransmisjon gjennom vegger, Sammenlikning av måledata og beregninger, Master's thesis, Norwegian Technical and Natural Science University, available from ⟨https://brage.bibsys.no/xmlui/handle/11250/233013⟩, in Norwegian, 2014.